ADVANCES IN ATMOSPHERIC SCIENCES, VOL. 39, JULY 2022, 1184–1197

• **Original Paper** •

Influence of South Asian Biomass Burning on Ozone and Aerosol Concentrations Over the Tibetan Plateau※

Junhua YANG[1], Shichang KANG*[1,2,3], Yuling HU[1], Xintong CHEN[1,2], and Mukesh RAI[1,2]

[1]*State Key Laboratory of Cryospheric Science*, *Northwest Institute of Eco-Environment and Resources*, *Chinese Academy of Sciences (CAS)*, *Lanzhou* 730000, *China*

[2]*University of Chinese Academy of Sciences*, *Beijing* 100049, *China*

[3]*CAS Center for Excellence in Tibetan Plateau Earth Sciences*, *Beijing* 100101, *China*

(Received 28 May 2021; revised 19 January 2022; accepted 11 February 2022)

ABSTRACT

In this work, the influence of South Asian biomass burning emissions on O_3 and $PM_{2.5}$ concentrations over the Tibetan Plateau (TP) is investigated by using the regional climate chemistry transport model WRF-Chem. The simulation is validated by comparing meteorological fields and pollutant concentrations against in situ observations and gridded datasets, providing a clear perspective on the spatiotemporal variations of O_3 and $PM_{2.5}$ concentrations across the Indian subcontinent, including the Tibetan Plateau. Further sensitivity simulations and analyses show that emissions from South Asian biomass burning mainly affect local O_3 concentrations. For example, contribution ratios were up to 20% in the Indo-Gangetic Plain during the pre-monsoon season but below 1% over the TP throughout the year 2016. In contrast, South Asian biomass burning emissions contributed more than 60% of $PM_{2.5}$ concentration over the TP during the pre-monsoon season via significant contribution of primary $PM_{2.5}$ components (black carbon and organic carbon) in western India that were lofted to the TP by westerly winds. Therefore, it is suggested that cutting emissions from South Asian biomass burning is necessary to alleviate aerosol pollution over the TP, especially during the pre-monsoon season.

Key words: South Asian biomass burning, ozone, aerosol, black carbon, Tibetan Plateau

Citation: Yang, J. H., S. C. Kang, Y. L. Hu, X. T. Chen, and M. Rai, 2022: Influence of South Asian biomass burning on ozone and aerosol concentrations over the Tibetan Plateau. *Adv. Atmos. Sci.*, **39**(7), 1184–1197, https://doi.org/10.1007/s00376-022-1197-0.

Article Highlights:

- South Asian biomass burning markedly affects aerosol load over the Tibetan Plateau.
- South Asian biomass burning contributes very little O_3 over the Tibetan Plateau.
- Carbonaceous aerosols from western India can be lofted to the Tibetan Plateau.

1. Introduction

Biomass burning, including the combustion of natural (e.g., wildfires) and prescribed (e.g., residential wood combustion in fireplaces) vegetation, releases large amounts of trace gases (e.g., CO, NO_x, and CH_4) and aerosols, which have gradually affected air quality (Bran et al., 2017), climate change by perturbing the radiation budget (Jacobson, 2014), as well as human health (Venkataraman et al., 2005). Emissions of biomass burning have been found to be a crucial contributor causing atmospheric pollution in South Asia (Streets et al., 2003). For example, annual biomass burning emissions have reached up to 350 Tg in India (Venkataraman et al., 2006), contributing approximately one fourth of the total CO and NO_x emissions in the Indian subcontinent (Venkataraman et al., 2006; Jena et al., 2015). Therefore, being adjacent to South Asia, the Himalayas and Tibetan Plateau (TP) are highly susceptible to trans-boundary atmospheric pollutants from South Asian biomass burning that affect their vulnerable environments, particularly cryospheric environments.

The Himalayas and TP, known together as a water tower for surrounding regions and having the largest ice mass outside the Arctic and Antarctica (Barnett et al., 2005; Yao et al., 2007, 2015), are the source of the headwaters of many major rivers in Asia, such as the Yangtze River, Yellow River, and Mekong River (Fekete et al., 1999; Xu et al.,

※ This paper is a contribution to the special issue on Third Pole Atmospheric Physics, Chemistry, and Hydrology.

* Corresponding author: Shichang KANG
Email: Shichang.kang@lzb.ac.cn

2008). Satellite-based aerosol optical depth images have clearly shown high concentration levels of air pollutants extending from South Asia and accumulating on the southern slope of the Himalayas, then overflowing into the TP region (Ramanathan et al., 2005; Seinfeld, 2008; Kang et al., 2019). Moreover, in situ observations have substantiated the hypothesis that pollutants from South Asia can be transported to the inner TP via the westerlies and Indian monsoon (Xu et al., 2009; Xia et al., 2011; Li et al., 2016). The back-trajectory analysis method also confirmed the pollutant transmission from South Asia to the Himalayas and Tibetan Plateau (Lu et al., 2012; Chen et al., 2018). By numerical modeling analysis, South Asia anthropogenic emissions were found to contribute 61.3% of black carbon over the TP during the non-monsoon season (Yang et al., 2018a). Nonetheless, the aforementioned studies overlook the influence of biomass burning emissions from South Asia on atmospheric pollution and their climatic/hydrospheric effects over the TP.

Compared with a large number of studies conducted on other regions of the world, only a few studies have focused on the impact of biomass burning over South Asia and adjacent regions. Analysis of in situ measurements indicates that biomass burning from India evidently affects air quality in the national capital city Delhi (Ghude et al., 2008), western India (Beig et al., 2008), northeast India (Deka and Hoque, 2014; Rajput et al., 2014), and central Himalayas (Kumar et al., 2011) during the pre-monsoon season. Cong et al. (2015) found that biomass burning emissions from South Asia were closely related to organic aerosols on both slopes of the Himalayas, transported there by large-scale atmospheric circulation and a unique mountain/valley breeze system. Li et al. (2016) used the source-diagnostic $\Delta^{14}C/\delta^{13}C$ method to ascertain that the biomass burning from the Indo–Gangetic Plain significantly contributes to black carbon (BC) aerosol at specific sites over the TP; similar results were also reported by Xu et al. (2013). High-temporal-resolution measurements of particulate chemical compositions show that air pollutants from South Asian biomass combustion can be transported to Mt. Yulong and the southeastern TP (Zheng et al., 2017). However, the in situ observational records are too sparse to effectively quantify the South Asian biomass burning's influence on the atmospheric chemical composition and air quality over the TP.

Some recent studies have conducted chemical transport modeling to investigate and evaluate the impact of South Asian biomass burning on regional O_3 and aerosol concentrations. Jane et al. (2015) investigated the impact of springtime biomass burning on regional O_3 distribution in South Asia by using the Weather Research and Forecasting model coupled with chemistry (WRF-Chem). Xu et al. (2018) applied the WRF-Chem model to study the regional BC distribution caused by biomass burning emissions from South Asia for two days. However, both existing WRF-Chem modeling studies were focused on very short time scales and do not reveal seasonal variation characteristics. In the present study, WRF-Chem simulations are performed for a whole year to provide detailed temporal and spatial distribution information for O_3 and aerosol concentrations over South Asia and the TP. Further, by performing sensitivity simulation experiments, we quantify the contribution of South Asian biomass burning to O_3 and various aerosol components and explicate their transportation mechanisms to the TP.

2. Method and data

2.1. *Simulation setup and design*

WRF-Chem, a newly developed regional dynamical/chemical transport model, involves complex physical and chemical processes and simulates the gas-phase chemical and aerosol microphysical processes on-line with the meteorological fields (Grell et al., 2005). It is capable of modeling regional air quality and has been successfully used for South Asia and the TP (Gao et al., 2015; Bran and Srivastava, 2017; Xu et al., 2018; Yang et al., 2018a, 2021). WRF-Chem v3.9.1 is used in this study. The key physical schemes consist of the Morrison 2-moment microphysical parameterization (Morrison et al., 2009), the RRTMG radiation schemes (Iacono et al., 2008), the Noah–MP land surface model (Niu et al., 2011), and the Yonsei University (YSU) planetary boundary layer scheme. The Carbon Bond Mechanism Version Z (CBMZ; Zaveri and Peters, 1999) is used for gas-phase chemical reaction. Aerosol reaction is based on the Model for Simulating Aerosol Interactions and Chemistry (MOSAIC; Zaveri et al., 2008), where the aerosol particle is divided into four bins.

The model domain has 25-km grid spacing (Fig. 1) and covers South Asia and the TP, with 155 and 135 grid cells in the west–east and north–south directions, respectively. The vertical configuration of the model includes 35 vertical sigma layers at the top pressure of 50 hPa. All grids are mapped on a Lambert projection, centered at 80°E, 26°N. National Centers for Environmental Prediction Final (NCEP FNL) analysis data with a horizontal resolution of 1° × 1° at 6-h time intervals is used for the meteorological initial and boundary conditions. The anthropogenic emissions are based on a global emissions inventory produced by Peking University at a resolution of 0.1°×0.1° (http://inventory.pku.edu.cn/) for the year 2014, including residential, industrial, transportation, energy production, as well as agriculture emission sources. The open biomass burning emissions are obtained from the fire inventory from NCAR (FINN), which is based on satellite observations (Wiedinmyer et al., 2011). The FINN inventory provides high-resolution data of open fires at 1-km spatial resolution and hourly temporal intervals; it includes wild fires, agricultural fires, and prescribed burnings. Finally, the output of Model for Ozone and related chemical Tracers (MOZART) is used to update the initial O_3 condition and the lateral boundary chemical conditions.

To investigate the influence of South Asian biomass burning on O_3 and aerosol concentrations over the TP, two

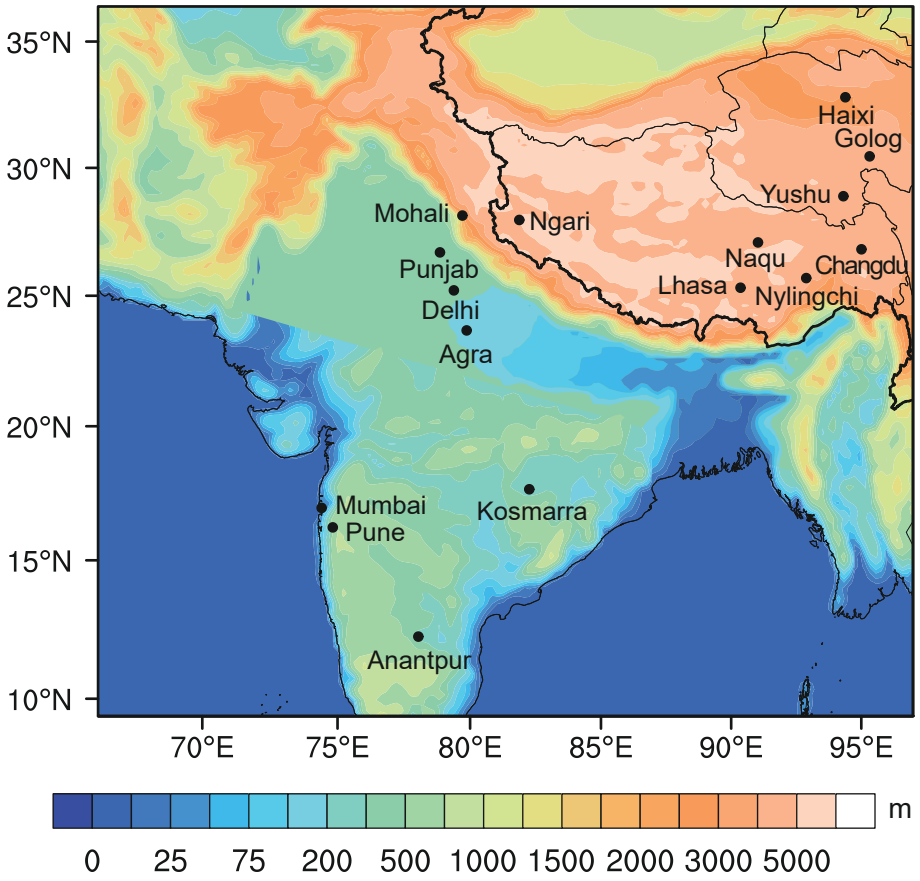

Fig. 1. WRF-Chem modeling domain, topographic field (m), and measured sites marked with black dots.

simulation experiments were conducted in this study. In the baseline simulation experiment, the original emissions of air pollutants from anthropogenic sources and open biomass burning were unchanged. In the sensitivity simulation, the biomass burning emissions of pollutants were set to zero over South Asia, including India, Pakistan, Nepal, Bhutan, and Bangladesh. These simulations were conducted for an entire year, from 1 December 2015 to 30 December 2016. The first month was considered the model spin-up time and was not analyzed. The seasonal average pollutant concentrations and meteorological elements during the pre-monsoon season (March to May), the monsoon season (June to September), the post-monsoon season (October to November), and winter (December, January, and February) were calculated from daily simulated results.

2.2. *Data*

Datasets from the Climate Research Unit (CRU; Mitchell and Jones, 2005, https://crudata.uea.ac.uk/cru/data/hrg/) provided by the UK's National Centre for Atmospheric Science, which are the most widely used observed climate datasets, were used to validate the model performance for surface temperature (T2). Simulated relative humidity (RH) and wind speed at 500 hPa were evaluated against the ERA-Interim reanalysis dataset obtained from the European Centre for Medium-Range Weather Forecasts (ECMWF, Dee et al., 2011, http://apps.ecmwf.int). The real-time daily concentrations of $PM_{2.5}$ and O_3 at eight sites were downloaded from the website of China National Environmental Monitoring Centre (http://106.37.208.233:20035) and were used for the assessment of simulation precision. In addition, we collected surface measurements of monthly average O_3 (Anantapur, Pune, Delhi, and Modal) and $PM_{2.5}$ (Agra, Mumbai, Kosmarra, and Punjab) concentrations over South Asia for the comparison with model simulation results. Detailed information about the measurements over South Asia is shown in Table S1. These air quality monitoring sites are distributed throughout the TP and South Asia and represent a wide range of environmental topography, including urban sites (Lhasa, Delhi, Agra, and Anantapur), semi-urban sites (Pune and Mohali), rural sites (Kosmarra and Punjab), coastal site (Mumbai), and other sites on the TP (Guolog, Haixi, Yushu, Ngari, Qamdo, Nylingchi and Nagqu). Figure 1 shows the locations of these monitoring sites.

3. Results and discussion

3.1. *Model evaluation*

3.1.1. *Meteorology*

In this work, we compared the simulated T2, as well as

RH and wind field at 500 hPa, with the CRU and ERA-interim reanalysis datasets (Fig. 2). The WRF-Chem model represents the spatial distribution pattern of annual T2 well (Fig. 2a). Warmer regions appeared in South Asia

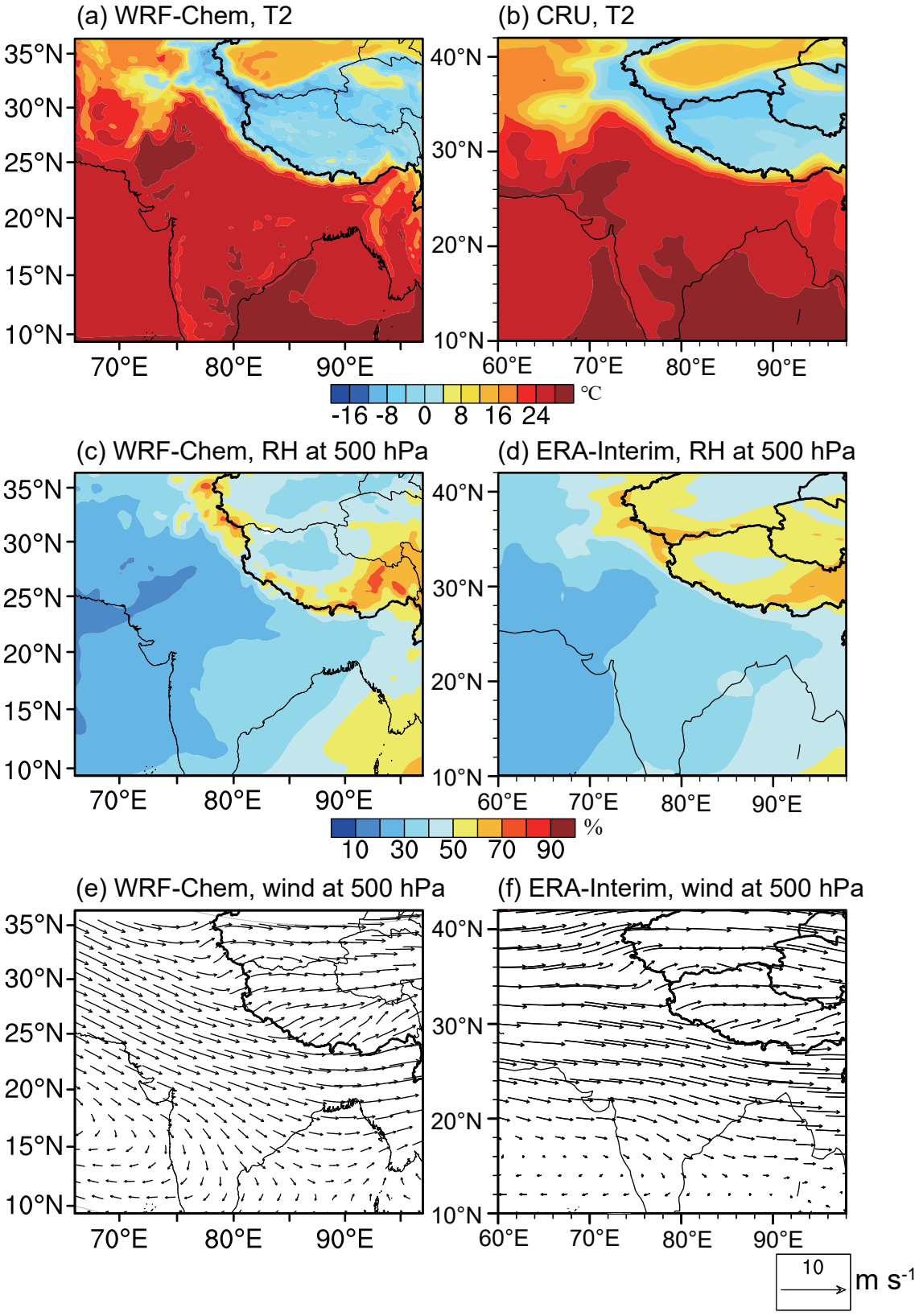

Fig. 2. Comparisons of annual T2, as well as RH and wind at 500 hPa between the WRF-Chem simulation and the reanalysis datasets.

(T2s>20°C), but colder regions appeared over the TP (T2s<0°C). Compared with the CRU (Fig. 2b), WRF-Chem captured the topographically induced variation of T2 over the TP in more detail, owing to its higher spatial resolution. Both WRF-Chem and ERA-interim results indicate that high 500-hPa RH occurred over the TP, but RH was relatively lower in South Asia (Figs. 2c and d). The model predicted slightly lower RH at 500 hPa over the northern TP compared with ERA-interim, which could be because of the simulation bias in temperature affecting the saturation pressure of water vapor (Yang et al., 2018b). The model also effectively reproduced the dynamics for the wind field at 500 hPa. There were prevailing westerly winds over the northern TP and southwesterly winds over the southern TP (Figs. 2e and f). Over South Asia, westerly winds from land to ocean were predominant. Overall, this simulation configuration captured the meteorological fields well, which is crucial to assure prediction accuracy of air pollutant concentrations.

Further, we quantitatively evaluated the model performance by using observations at stations in the study area (Fig. S1a in the Electronic Supplementary Material, ESM). The WRF-Chem model generally represents the correct annual variation trends of temperature and humidity at the stations. Compared with the observation, the model simulated higher T2 from June to September and slightly lower values in other months (Fig. S1b). On the other hand, the model simulated lower 2-m relative humidity than the observation from June to September (Fig. S1c). The corresponding statistics between WRF-Chem simulations and in situ observations are presented in Fig. S1.

3.1.2. *O_3 and aerosol*

We summarized surface O_3 (Fig. 3a) and $PM_{2.5}$ (Fig. 3b) concentrations from 12 sites to compare with the simulation results. The observed results show very high O_3 concentrations at TP sites. As in Haizi, Yushu, and Ngari, surface O_3 concentrations exceeded 100 μg m^{-3} in the pre-monsoon months. However, low O_3 levels appeared over South Asia, such as in Delhi (below 30 μg m^{-3}), at 1–2 orders of magnitude less than those over the TP sites. The simulation reflects the spatial variability of O_3 concentrations from the TP to South Asia. When the monthly variation of O_3 is considered, its concentration is found to have been lowest during the monsoon months over the TP. This might be because pollutants experience the washout effect in the rainy months (Yin et al., 2017). Moreover, the sky was always overcast during the monsoon season, thus, lower solar flux weakened the photochemical processes (Reddy et al., 2008). O_3 concentration was also lowest during the summer months at sites over South Asia. The highest O_3 concentration was found in May at Delhi and Mohali, partly owing to low humidity and high concentration of precursors (Lamaud et al., 2002). The model exhibited the annual trends of O_3 concentrations well at all TP sites, except for Haixi. Overestimation of O_3 concentration occurred in spring and underestimation occurred in autumn at Yushu, Ngari, Qamdo, Lhasa, and Nyingchi. The O_3 concentration was uniformly underpredicted at other TP sites, such as Guolog, Haixi, and Nagqu. In South Asia, the seasonal trend of O_3 concentration was reproduced well at all sites, despite a slight overestimation.

The model also represented the spatiotemporal variation of $PM_{2.5}$ concentrations well at all sites (Fig. 3b). Both the observation and simulation showed lower $PM_{2.5}$ over the TP (e.g., in Yushu and Lhasa) and higher $PM_{2.5}$ at sites over South Asia (e.g., in Agra and Kosmarra), which is opposite to the spatial variability of O_3 concentration from the TP to South Asia. Simulated $PM_{2.5}$ concentrations showed underestimations compared to in situ observations over the TP. However, it should be noted that there is uncertainty in the emissions inventory. For example, in Lhasa, the underestimation of residential emissions was considered as a crucial factor causing the underestimation of $PM_{2.5}$ (Li et al., 2019). The temporal variability of $PM_{2.5}$ concentration was reproduced well over the TP, with higher concentration values in winter months but lower values in summer. However, at Haixi and Guolog, $PM_{2.5}$ concentration reached its peak in May (42 μg m^{-3}) and June (43.5 μg m^{-3}), respectively, possibly due to westerly winds bringing dust to those locations during this period (Jia et al., 2015). High $PM_{2.5}$ concentrations were observed at sites over South Asia, which is one of the most densely populated regions in the world and has high local emission sources including household, vehicular, mining, and urbanization (Nair et al., 2007). Both observed and simulated $PM_{2.5}$ concentrations reached their maximum values during winter months and reached their minimums during summer months over South Asia, except at Punjab. The model accurately captures the highest $PM_{2.5}$ concentration in April (101.1 μg m^{-3}) at Punjab, which could be caused by agricultural waste burning emissions (Kharol et al., 2012). April in Punjab, India happens to be the start of one growing season and end of another, so crop residue burning was prevalent there. As seen in Fig. S2 in the ESM, the pre-monsoon $PM_{2.5}$ emissions from deforestation and wildfires increased significantly in western India, compared with other seasons.

Table 1 summarizes the model statistics of O_3 and $PM_{2.5}$ concentrations at the observed sites, including mean observation (OBS), mean simulation (SIM), normalized mean bias (NMB), and normalized mean error (NME). The performance criteria (NMB <±30%, NME <50%) for $PM_{2.5}$ and the performance criteria (NMB <±15%, NME <25%) for O_3 are suggested by Emery et al. (2001). Overall, the model statistics for O_3 and $PM_{2.5}$ in the region meet the model performance criteria. There are large underestimations of $PM_{2.5}$ in Guolog and Nagqu, partly because the model grid represents a regional average, but also, the observation site is intensely affected by local anthropogenic emissions such as industrial facilities and traffic. In addition, the model generally reflects the O_3 and $PM_{2.5}$ concentrations at these sites during the pre-monsoon season, with R^2 values of 0.89 for $PM_{2.5}$ and 0.81 for O_3 (Fig. S3 in the ESM), respectively.

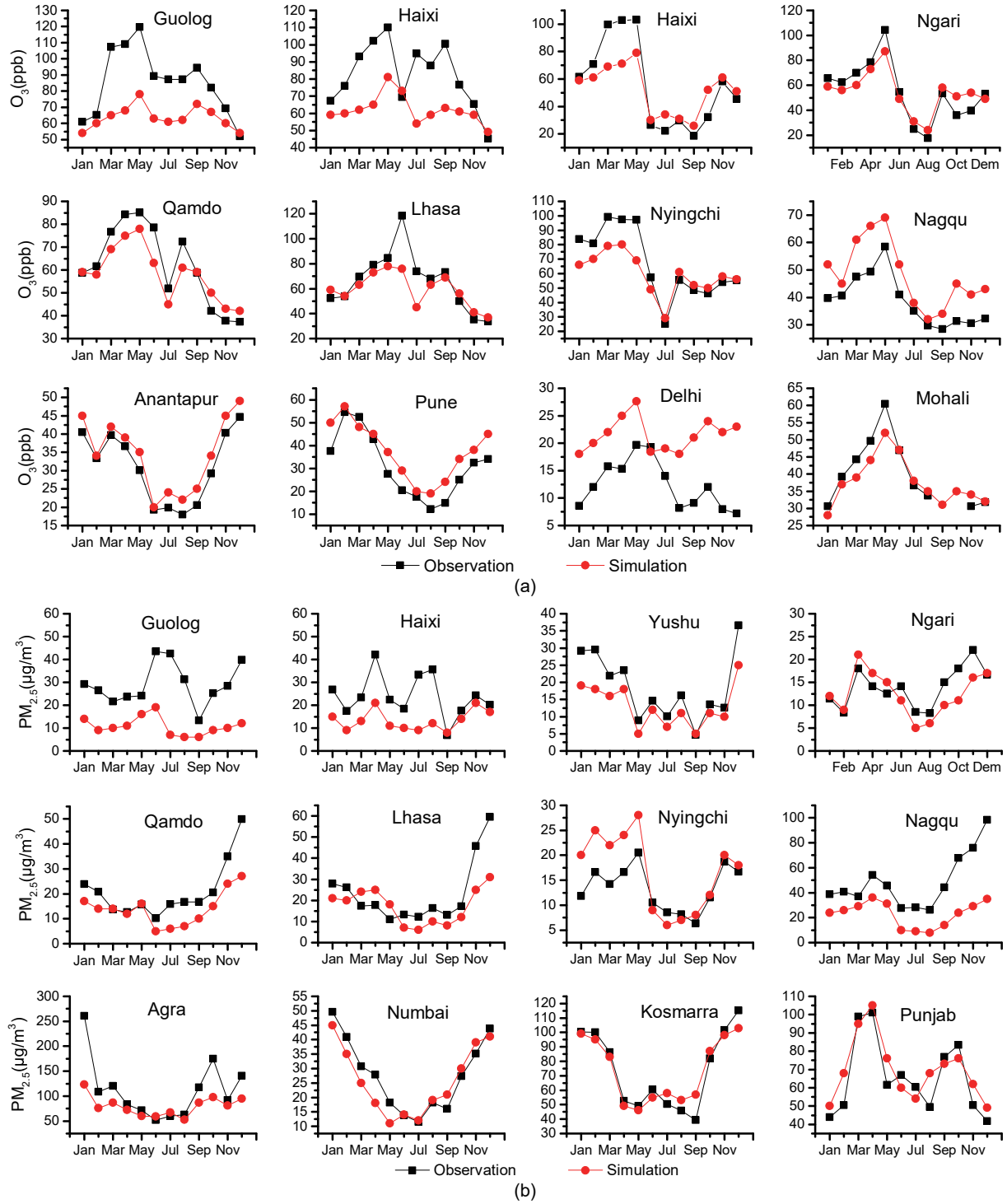

Fig. 3. The seasonal variations of observed and simulated O_3 (a) and $PM_{2.5}$ (b) concentrations at sites.

3.2. *Seasonal variations and regional distributions of O_3 and aerosol*

Figures 4a–d show the seasonal and spatial variations of simulated surface O_3 concentration. O_3 concentration was found to be higher over the TP but lower in South Asia, because of more intense photochemical reactions and downward transport of stratospheric air mass over the TP (Yin et al., 2017). Seasonally, higher O_3 concentrations occurred in the pre-monsoon season over the TP (Fig. 4a), likely owing to stronger stratosphere–troposphere exchange during this pre-monsoon season compared with other seasons (Yin et al., 2017). O_3 concentration declined to its minimum during the monsoon season over the TP (Fig. 4b), consistent with previous in situ observations (Lin et al., 2015; Yin et al., 2019). Since the greatest precipitation occurs during the monsoon season (Fig. S4 in the ESM), O_3 and its precursors

could be removed, thus reducing photochemistry and O_3 concentration over the TP (Ma et al., 2014). As for South Asia, surface O_3 concentrations are higher over northeastern India during all seasons except for the monsoon season, which may be attributed to higher O_3 precursor concentrations in this region, such as CO (Fig. S5 in the ESM).

Figures 4e–h illustrate the seasonal and spatial variation of surface $PM_{2.5}$ concentrations. $PM_{2.5}$ concentration is observed to be high in eastern and northeastern regions of South Asia during the pre-monsoon season (Fig. 4e), possibly due to the local forest fires. As seen in Fig. S2, $PM_{2.5}$ emissions from deforestation and wildfires in eastern South Asia were significantly greater during the pre-monsoon season than during other seasons. Meanwhile, higher $PM_{2.5}$ concentrations appeared over the TP during the pre-monsoon season compared with other seasons; this was accompanied with a decreasing trend from the southwest TP to the northeast TP. There are very little local emissions over the TP,

Table 1. Model performance for O_3 and $PM_{2.5}$ concentrations at sites. OBS is mean observation; SIM is mean simulation; NMB is Normalized mean bias; NME is Normalized mean error. The performance criteria (NMB <±30%, NME <50%) for $PM_{2.5}$ and the performance criteria (NMB <±15%, NME <25%) for O_3 are suggested by Emery et al. (2001). The values that do not meet the criteria are marked in bold.

	O_3					$PM_{2.5}$				
	Obs	Sim	NMB	NME	*R*	Obs	Sim	NMB	NME	*R*
Guolog	85.3	66.7	−14.4	23.8	0.86	29.1	13.7	**−36.9**	36.9	0.71
Haixi	82.4	64.1	−12.9	21.1	0.74	24.0	16.8	−28.1	43.7	0.76
Yushu	55.9	52	−6.9	22.6	0.93	18.4	13.1	−29.1	29.3	0.97
Mgaro	54.9	54.2	−1.4	15.7	0.94	13.9	12.5	−10.2	21.9	0.77
Qamdo	62.1	58.5	−5.8	10.7	0.89	20.9	14.5	−28.5	34.1	0.86
Lhasa	65.9	59.5	−9.7	15.4	0.80	23.1	17.3	−25.4	40.4	0.73
Nylingchi	66.7	59.9	−10.1	15.5	0.92	13.4	16.6	24.2	30.6	0.89
Nagqu	38.6	44.2	12.5	14.5	0.91	48.7	32.9	**−32.9**	32.9	0.72
Pune	30.9	37.1	13.8	22.5	0.94	–	–	–	–	–
Delhi	16.4	21.5	12.3	21.4	0.76	–	–	–	–	–
Anantapur	31.0	34.5	11.3	11.3	0.98	–	–	–	–	–
Mohali	40.4	37.6	4.4	7.6	0.95	–	–	–	–	–
Agra	–	–	–	–	–	112.0	79.8	−28.7	30.8	0.95
Mumbai	–	–	–	–	–	27.7	25.8	−6.9	14.7	0.92
Kosmarra	–	–	–	–	–	73.6	72.5	−1.8	8.6	0.96
Punjab	–	–	–	–	–	65.4	69.7	6.4	13.7	0.88

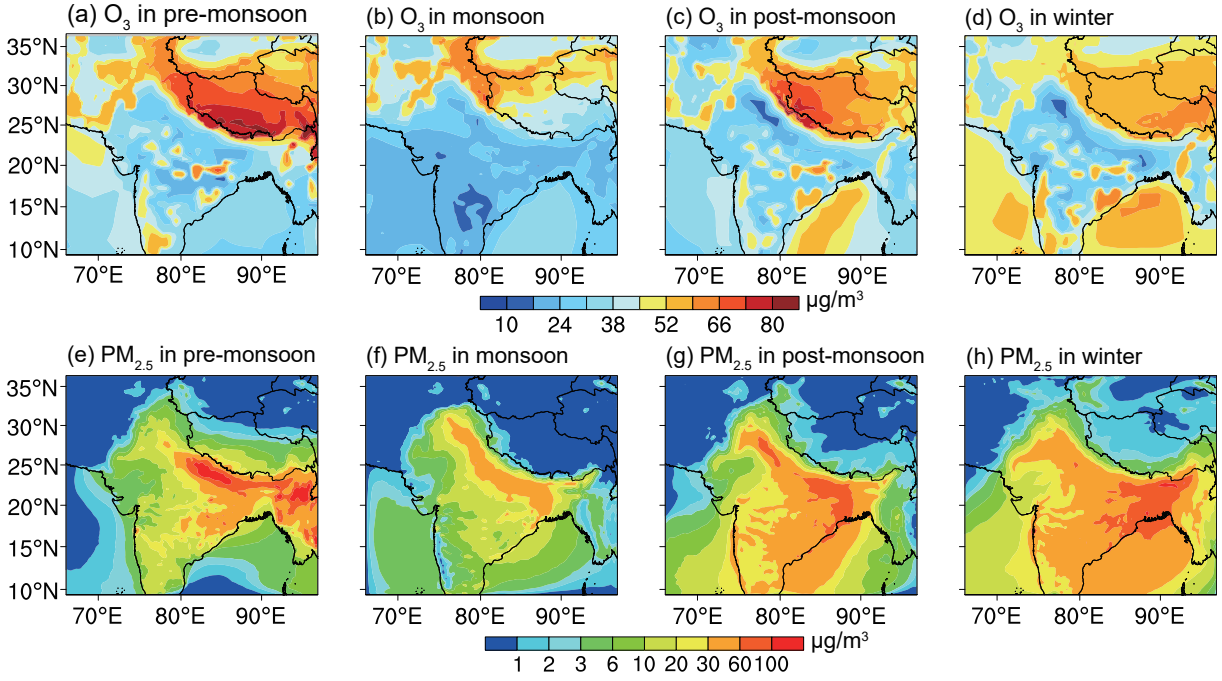

Fig. 4. The seasonal and regional variations of predicted O_3 and $PM_{2.5}$ concentrations.

and westerly winds prevail during the pre-monsoon season. Thus, high $PM_{2.5}$ mass over the TP during the pre-monsoon season probably was caused by the cross-border transmission from western India. The lowest $PM_{2.5}$ concentrations (below 60 μg m^{-3}) are observed during the monsoon season (Fig. 4f) because the large amount of precipitation (Fig. S4) in this season leads to intense wet scavenging of particulate matter. $PM_{2.5}$ concentration is found to be high over the southern Indian subcontinent during the post-monsoon season (Fig. 4g) and winter (Fig. 4h) because low wind speeds at the surface (Fig. S6 in the ESM) as well as little precipitation (Fig. S4) are unfavorable to pollutant diffusion and dispersion. Higher $PM_{2.5}$ concentrations occurred over the TP during the post-monsoon season and winter compared with the monsoon season, which is partly because of stagnant meteorological conditions during the post-monsoon season and winter, i.e., less precipitation (Fig. S4d) and lower wind speeds (Fig. S6d); it is also partly because of the cross-border transmission by the large-scale air circulation and regional mountain–valley wind.

The spatial distributions of $PM_{2.5}$ components had significant seasonal variations (Fig. 5). Secondary inorganic components (SO_4, NO_3, and NH_4) showed higher concentration values during the post-monsoon season and winter over South Asia, whereas the concentrations were lower during the monsoon season. Increasing residential emissions of SO_2 and NO_x during winter (Fig. S7 in the ESM) resulted in an increase of surface heterogeneous reactions for the formation of SO_4 and NO_3 in this period. The NO_3 to SO_4 mass ratio refers to the relative dominance of stationary versus mobile emission sources (Wan et al., 2016). The NO_3/SO_4 mass ratios below 1 in India during the pre-monsoon season indicate that the mobile emissions are not the main source there. Besides, colder weather in winter is more preferential to ammonium nitrate being partitioned into the particle phase (Aw and Kleeman, 2003). Primary $PM_{2.5}$ component (BC and OC) concentrations over the TP reached their highest values during the pre-monsoon season (Figs. 5m and q) due to the cross-border transmission. High primary component concentrations occurred over the Indian subcontinent during winter (Figs. 5p and t), driven by the significant increase of residential emissions during winter, as well as stagnant weather conditions as discussed above.

Winter SO_4, NO_3, and NH_4 concentrations were 50%–250% higher than the annual average concentrations in southern India and the Bay of Bengal (Fig. S8 in the ESM). However, winter SO_4 concentration is lower than the annual mean over the TP, where NO_3 and NH_4 do not evidently deviate from the average. During the pre-monsoon season, secondary inorganic components are 50%–100% higher than the annual mean over the western TP (Figs. S8a, c, and e). As for primary components over the TP and its southern slope, BC concentration is 50%–200% higher during the pre-monsoon season than its annual mean, while OC concentration during the pre-monsoon season is approximately 100%-250% higher than its annual mean (Fig. S9 in the ESM). Higher BC and OC concentrations during the pre-monsoon season indicate that primary components were the more vital contributor to the maximum $PM_{2.5}$ concentrations over the TP during the pre-monsoon season. Moreover, maximum $PM_{2.5}$ concentrations in the northern Indo-Gangetic plain and the Himalayan foothills could be attributable to the primary components which are approximately 100-150% of the annual mean, whereas secondary inorganic components are lower than their annual means during the pre-monsoon season (Fig. S8).

3.3. *Effects of South Asian biomass burning on O_3 and aerosol concentrations*

In sections 3.1 and 3.2, we validated the WRF-Chem performance for meteorological fields, O_3, and aerosol, using in situ observations and gridded data. The results suggest that this model framework is capable to further quantify the contribution proportion of South Asian biomass burning to O_3 and aerosol concentrations. The contribution proportion is calculated by $(A–W)/A$, where A and W are pollutant concentration in the sensitivity and control simulations, respectively.

3.3.1. *O_3*

Biomass burning emissions affect O_3 concentration mainly by influencing the emissions of O_3 precursors (Andreae and Merlet, 2001). Figure 6 illustrates the contribution ratios of South Asian biomass burning to O_3 concentrations during different seasons. South Asian biomass burning contributes to O_3 primarily in South Asia, especially during the pre-monsoon season (Fig. 6a) and winter (Fig. 6d). This is because South Asian biomass burning significantly influences O_3 precursors in South Asia, particularly CO (Fig. S10 in the ESM). During the pre-monsoon season, higher contribution ratios (up to 20%) of South Asian biomass burning to O_3 concentration appeared in the Indo-Gangetic Plain and central India (Fig. 6a), which experience a large number of fire counts in this period (Xu et al., 2018). However, South Asian biomass burning contributed less than 1% of the O_3 concentration over the TP during the pre-monsoon season, although the biomass burning from western India reached its maximum and westerly winds prevailed during the pre-monsoon season (Fig. S6a). Therefore, it can be inferred that high O_3 concentration over the TP during the pre-monsoon season (Fig. 4a) is mainly a result of local weather and environmental factors such as strong stratosphere–troposphere exchange and high background concentration of O_3. South Asian biomass burning has very little influence on O_3 concentration during the monsoon season (Fig. 6b). During the post-monsoon season, high contribution proportion of South Asian biomass burning to O_3 concentration was mainly concentrated in western India (Fig. 6c). Compared with that during the post-monsoon season, the fires from South Asia showed a larger contribution to O_3 concentration in south India during winter (Fig. 6d), consistent with more fire counts in this region during winter.

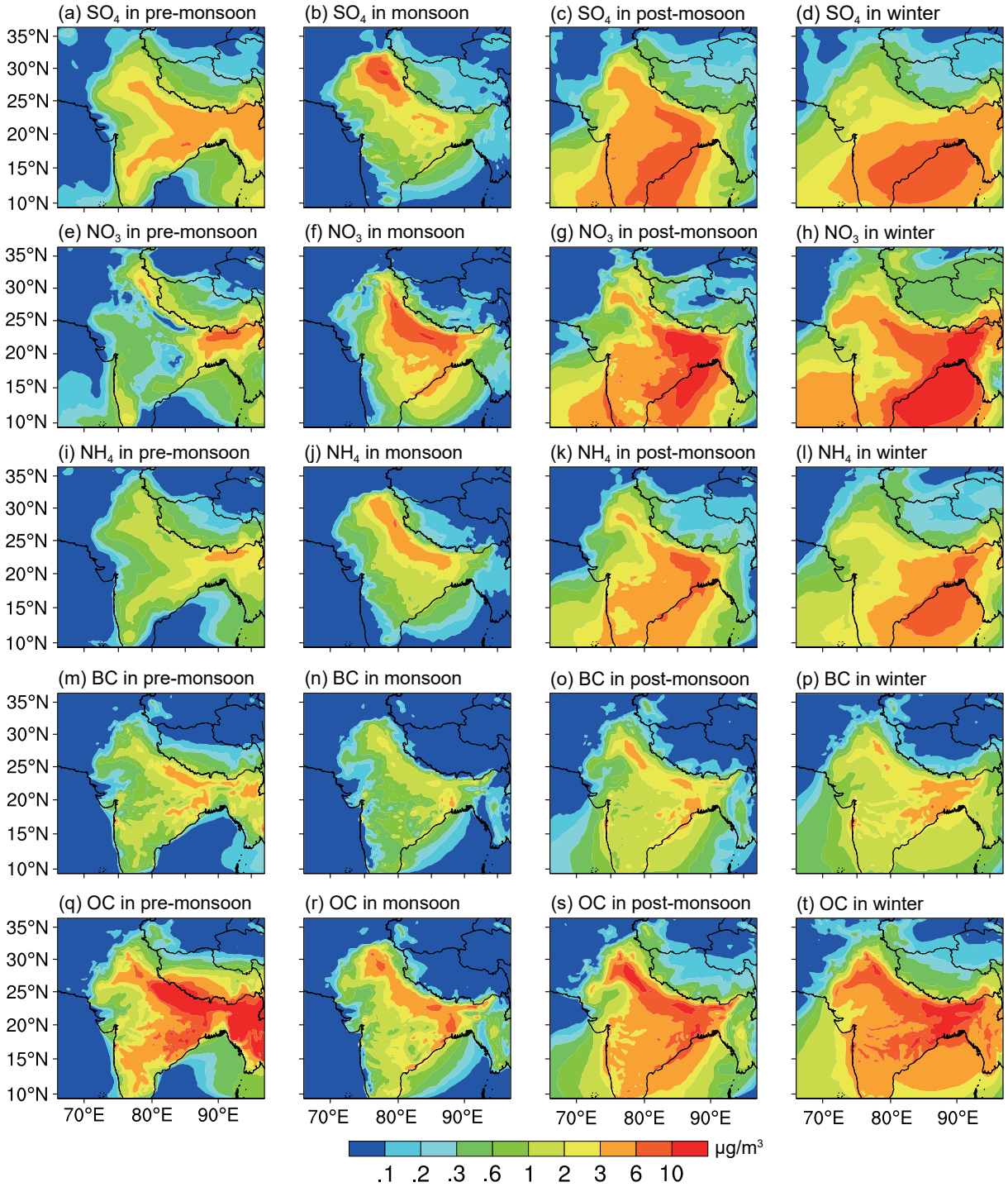

Fig. 5. The seasonal and regional variations of predicted $PM_{2.5}$ components.

3.3.2. *$PM_{2.5}$ and its components*

Figure 7 shows the contribution ratios of South Asian biomass burning to $PM_{2.5}$ and its components. During the pre-monsoon season, high contribution proportions (more than 60%) were observed over the TP and its southern slope (Fig .7a), coincident with the regions with highest $PM_{2.5}$ concentration during the pre-monsoon season (Fig. 7e). This is primarily because South Asian biomass burning contributed significantly to primary $PM_{2.5}$ components [BC (Fig. 7q) and OC (Fig. 7u)] over the TP and northern Indo-Gangetic plains during the pre-monsoon season. Moreover, the contribution ratios to primary components showed a gradual decreasing trend from the western TP to eastern TP. Considering that there are very few local emissions over the TP, the primary components over the TP must be mainly transported from western India. As seen in Fig. S11, South Asian biomass burning caused a clear increase of BC (Fig. S11a in the ESM) and OC (Fig. S11b in the ESM) concentrations

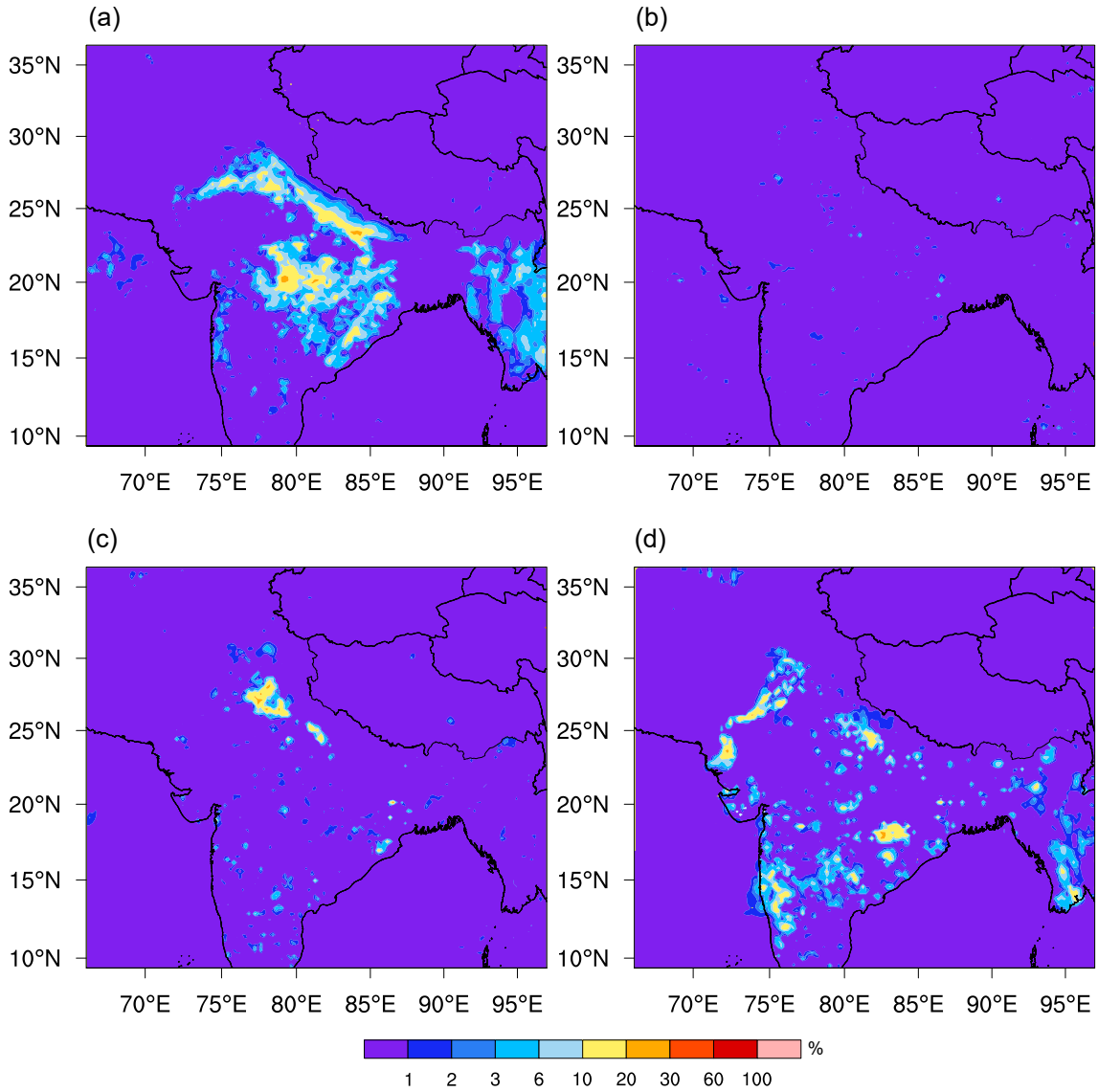

Fig. 6. The influence ratios of South Asian biomass burning to O_3 during different seasons: (a) pre-monsoon, (b) monsoon, (c) post-monsoon, (d) winter.

along the foothills of the Himalayas and the eastern part of the Indian subcontinent, and these pollutants can be transported there from western India by northwesterly and southwesterly winds. We then analyze the cross-border transmission of South Asian biomass burning emissions into BC (Fig. S11c) and OC (Fig. S11d) concentrations over the TP along 30°N, which shows BC and OC in western India can reach 500 hPa and then be transported onto the TP by the westerly winds.

Meanwhile, the South Asian biomass burning contribution to secondary inorganic components was less than 10% over the TP and northern Indo-Gangetic plains (Figs. 7e, i, and m). The insignificant contributions of South Asian biomass burning to secondary inorganic components of $PM_{2.5}$ could be attributed to its low contribution to the gaseous precursors of these secondary $PM_{2.5}$ components (Fig. S12 in the ESM). The only exception is the relatively higher contribution ratios of South Asian biomass burning to NO_3 concentrations over the Indian subcontinent in the pre-monsoon season (Fig. 6i), which is due to the larger contribution of South Asian biomass burning to local NO_2 concentrations (Fig. S13 in the ESM).

The lowest contribution proportions of South Asian biomass burning to $PM_{2.5}$ mass and its components were found during the monsoon season, mainly because of the minimal biomass burning emissions in this season. During the post-monsoon season, South Asian biomass burning contributed up to 50% of the $PM_{2.5}$ mass in western India (Fig. 7c), owing to its significant contribution to BC (Fig. 6s) and OC (Fig. 7w) in this season. South Asian biomass burning also evidently affected the concentrations of primary $PM_{2.5}$ components over the TP during the post-monsoon season (Figs. 7s and w), with contribution ratios of more than 10%. However, South Asian biomass burning contributed less

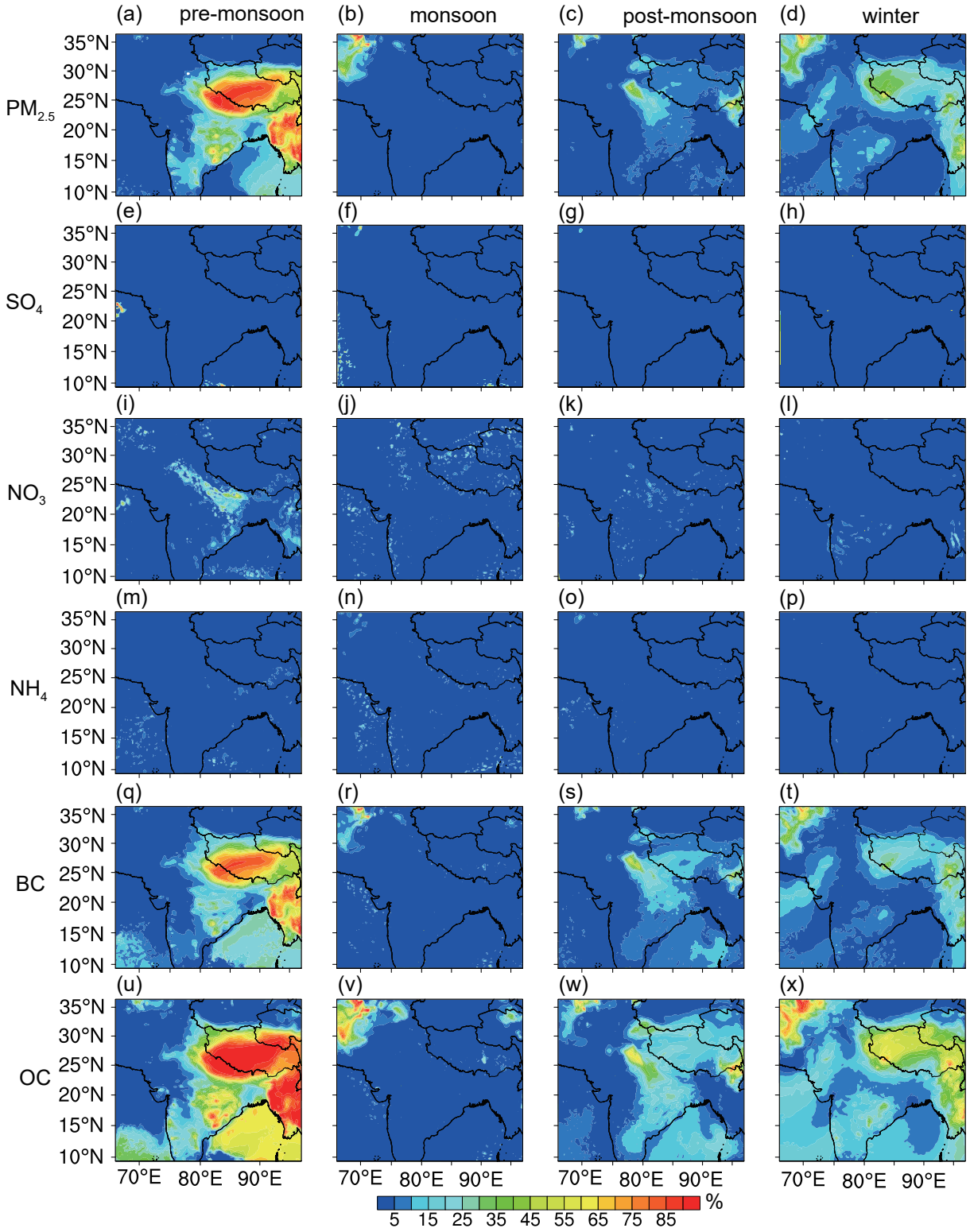

Fig. 7. The contribution ratios of South Asian biomass burning to $PM_{2.5}$ and its components during different seasons.

than 10% of the $PM_{2.5}$ over the TP in the post-monsoon season (Fig. 7c). It reflects that primary $PM_{2.5}$ components accounted for less $PM_{2.5}$ mass over the TP compared with secondary $PM_{2.5}$ components (SO_4, NO_3, and NH_4), which is consistent with higher concentrations of secondary components being present during the post-monsoon season (Figs. 5c, g, and k).

Although $PM_{2.5}$ concentration was higher over the southern Indian subcontinent during winter (Fig. 4h) than during the pre-monsoon season (Fig. 4e), South Asian biomass burning contributed less toward winter $PM_{2.5}$ there (Fig. 7d). This can be attributed to the same reason that South Asian bio-

mass burning contributed very little to primary (Fig. 7h) and secondary inorganic (Figs. 7h, l, and p) components over the Indian subcontinent during winter. It implies that the highest $PM_{2.5}$ concentration over the southern Indian subcontinent during winter (Fig. 4h) might be caused by other emission sources and stagnant weather conditions (less precipitation (Fig. S2d in the ESM) and low wind speed (Fig. S4d)). As shown in Fig. S14, residential and industrial emissions of $PM_{2.5}$ were significantly greater during winter in southern India.

4. Conclusions

In this study, O_3 and $PM_{2.5}$ over South Asia and the TP were simulated using WRF-Chem for the whole year of 2016. This simulation configuration provided an appropriate performance on meteorological conditions. The comparison of simulated and observed O_3 and $PM_{2.5}$ concentrations indicated that the model can represent O_3 and $PM_{2.5}$ well compared to most in situ observations for most months. The simulation results showed relatively higher O_3 concentrations over the TP during the pre-monsoon season and relatively lower concentrations during the monsoon season. In South Asia, higher O_3 concentrations in northeastern India during all seasons except for the monsoon season are closely related to higher O_3 precursor concentrations. Similarly, high $PM_{2.5}$ concentrations appeared in eastern and northeastern regions of South Asia. The $PM_{2.5}$ components had significant spatiotemporal variations. Primary $PM_{2.5}$ components were found to be more crucial to forming the highest $PM_{2.5}$ concentrations over the TP during the pre-monsoon season compared with secondary inorganic $PM_{2.5}$ components. In the northern Indo-Gangetic plains and the Himalayan foothills, secondary inorganic components during the pre-monsoon season are lower than their annual mean.

Finally, we calculated the South Asian biomass burning contribution to O_3 and $PM_{2.5}$ concentrations. The contribution of South Asian biomass burning to O_3 was mainly concentrated in South Asia, with the highest contribution ratios of up to 20% in the Indo-Gangetic Plain during the pre-monsoon season, but contributions were less than 1% over the TP throughout the year. By contrast, South Asian biomass burning contributed more than 60% of the $PM_{2.5}$ over the TP and its southern slope during the pre-monsoon season due to its significant contribution to primary $PM_{2.5}$ components (BC and OC) in western India, which can be lofted to the TP by the westerly winds. Therefore, cutting down South Asian biomass burning emissions is necessary to mitigate air pollution over South Asia and the TP, especially during the pre-monsoon season.

Acknowledgements. This study was supported by the National Natural Science Foundation of China (Grant Nos. 42071096 and 41901071), Second Tibetan Plateau Scientific Expedition and Research Program (STEP) (Grant No. 2019QZKK0605), State Key Laboratory of Cryospheric Science (Grant No. SKLCS-ZZ-2022), Strategic Priority Research Program of Chinese Academy of Sciences and the Open Program (Grant No. SKLCS 2020-10) from State Key Laboratory of Cryospheric Science, and Youth Science Foundation of Hebei Province (Grant No. D2019106042).

Electronic supplementary material: Supplementary material is available in the online version of this article at https://doi.org/10.1007/s00376-022-1197-0.

REFERENCES

Andreae, M. O., and P. Merlet, 2001: Emission of trace gases and aerosols from biomass burning. *Global Biogeochemical Cycles*, **15**, 955–966, https://doi.org/10.1029/2000GB001382.

Aw, J., and M. J. Kleeman, 2003: Evaluating the first-order effect of intraannual temperature variability on urban air pollution. *J. Geophys. Res.*, **108**(D12), 4365, https://doi.org/10.1029/2002JD002688.

Barnett, T. P., J. C. Adam, and D. P. Lettenmaier, 2005: Potential impacts of a warming climate on water availability in snow-dominated regions. *Nature*, **438**(7066), 303–309, https://doi.org/10.1038/nature04141.

Beig, G., S. D. Ghude, S. D. Polade, and B. Tyagi, 2008: Threshold exceedances and cumulative ozone exposure indices at tropical suburban site. *Geophys. Res. Lett.*, **35**, L02802, https://doi.org/10.1029/2007GL031434.

Bran, S. H., and R. Srivastava, 2017: Investigation of $PM_{2.5}$ mass concentration over India using a regional climate model. *Environmental Pollution*, **224**, 484–493, https://doi.org/10.1016/j.envpol.2017.02.030.

Chen, X. T., S. C. Kang, Z. Y. Cong, J. H. Yang, and Y. M. Ma, 2018: Concentration, temporal variation, and sources of black carbon in the Mt. Everest region retrieved by real-time observation and simulation. *Atmospheric Chemistry and Physics*, **18**(17), 12 859–12 875, https://doi.org/10.5194/acp-18-12859-2018.

Cong, Z., S. Kang, K. Kawamura, B. Liu, X. Wan, Z. Wang, S. Gao, and P. Fu, 2015: Carbonaceous aerosols on the south edge of the Tibetan Plateau: Concentrations, seasonality and sources. *Atmospheric Chemistry and Physics*, **15**, 1573–1584, https://doi.org/10.5194/acp-15-1573-2015.

Dee, D. P., and Coauthors, 2011: The ERA-interim reanalysis: Configuration and performance of the data assimilation system. *Quart. J. Roy. Meteor. Soc.*, **137**(656), 553–597, https://doi.org/10.1002/qj.828.

Deka, P., and R. R. Hoque, 2014: Incremental effect of festive biomass burning on wintertime PM_{10} in Brahmaputra Valley of Northeast India. *Atmospheric Research*, **143**, 380–391, https://doi.org/10.1016/j.atmosres.2014.03.003.

Emery, C., E. Tai, and G. Yarwood, 2001: Enhanced meteorological modeling and performance evaluation for two Texas ozone episodes. Project Rep. Prepared for the Texas Natural Resource Conservation Commission.

Fekete, B. M., C. J. Vörösmarty, and W. Grabs, 1999: Global composite runoff fields on observed river discharge and simulated water balances. Tech. Rep. No. 22, 115 pp.

Gao, Y., M. Zhang, Z. Liu, L. Wang, P. Wang, X. Xia, M. Tao, and L. Zhu, 2015: Modeling the feedback between aerosol and meteorological variables in the atmospheric boundary layer during a severe fog–haze event over the North China

Plain. *Atmospheric Chemistry and Physics*, **15**, 4279–4295, https://doi.org/10.5194/acp-15-4279-2015.

Ghude, S. D., S. Fadnavis, G. Beig, S. D. Polade, and A. R. J. van der, 2008: Detection of surface emission hot spots, trends, and seasonal cycle from satellite-retrieved NO_2 over India. *J. Geophys. Res.*, **113**, D20305, https://doi.org/10.1029/2007JD009615.

Grell, G. A., S. E. Peckham, R. Schmitz, S. A. McKeen, G. Frost, W. C. Skamarock, and B. Eder, 2005: Fully coupled "online" chemistry within the WRF model. *Atmos. Environ.*, **39**, 6957–6975, https://doi.org/10.1016/j.atmosenv.2005.04.027.

Iacono, M. J., J. S. Delamere, E. J. Mlawer, M. W. Shephard, S. A. Clough, and W. D. Collins, 2008: Radiative forcing by long-lived greenhouse gases: Calculations with the AER radiative transfer models. *J. Geophys. Res.*, **113**, D13103, https://doi.org/10.1029/2008JD009944.

Jacobson, M. Z., 2014: Effects of biomass burning on climate, accounting for heat and moisture fluxes, black and brown carbon, and cloud absorption effects. *J. Geophys. Res.*, **119**(14), 8980–9002, https://doi.org/10.1002/2014JD021861.

Jane, C. M., and Coauthors, 2015: Influence of springtime biomass burning in South Asia on regional ozone (O_3): A model based case study. *Atmospheric Environment*, **100**, 37–47, https://doi.org/10.1016/j.atmosenv.2014.10.027.

Jena, C., and Coauthors, 2015: Influence of springtime biomass burning in South Asia on regional ozone (O_3): A model based case study. *Atmos. Environ.*, **100**, 37–47, https://doi.org/10.1016/j.atmosenv.2014.10.027.

Jia, R., Y. Z. Liu, B. Chen, Z. J. Zhang, and J. P. Huang, 2015: Source and transportation of summer dust over the Tibetan Plateau. *Atmos. Environ.*, **123**, 210–219, https://doi.org/10.1016/j.atmosenv.2015.10.038.

Kang, S. C., and Coauthors, 2019: Linking atmospheric pollution to cryospheric change in the third Pole region: Current progress and future prospects. *National Science Review*, **6**, 796–809, https://doi.org/10.1093/nsr/nwz031.

Kharol, S. K., K. V. S. Badarinath, A. R. Sharma, D. V. Mahalakshmi, D. Singh, and V. K. Prasad, 2012: Black carbon aerosol variations over Patiala city, Punjab, India—A study during agriculture crop residue burning period using ground measurements and satellite data. *Journal of Atmospheric and Solar-Terrestrial Physics*, 84**–85**, 45–51, https://doi.org/10.1016/j.jastp.2012.05.013.

Kumar, R., and Coauthors, 2011: Influences of the springtime northern Indian biomass burning over the central Himalayas. *J. Geophys. Res.*, **116**, D19302, https://doi.org/10.1029/2010JD015509.

Lamaud, E., A. Carrara, Y. Brunet, A. Lopez, and A. Druilhet, 2002: Ozone fluxes above and within a pine forest canopy in dry and wet conditions. *Atmos. Environ.*, **36**, 77–88, https://doi.org/10.1016/S1352-2310(01)00468-X.

Li, C. L., and Coauthors, 2016: Sources of black carbon to the Himalayan–Tibetan Plateau glaciers. *Nature Communications*, **7**, 12574, https://doi.org/10.1038/ncomms12574.

Li, C. L., and Coauthors, 2019: Heavy near-surface $PM_{2.5}$ pollution in Lhasa, China during a relatively static winter period. *Chemosphere*, **214**, 314–318, https://doi.org/10.1016/j.chemosphere.2018.09.135.

Lin, W. L., X. B. Xu, X. D. Zheng, J. Dawa, C. Baima, and J. Ma, 2015: Two-year measurements of surface ozone at Dangxiong, a remote highland site in the Tibetan Plateau. *Journal of Environmental Sciences*, **31**, 133–145, https://doi.org/10.1016/j.jes.2014.10.022.

Lu, Z. F., D. G. Streets, Q. Zhang, and S. W. Wang, 2012: A novel back-trajectory analysis of the origin of black carbon transported to the Himalayas and Tibetan Plateau during 1996–2010. *Geophys. Res. Lett.*, **39**, L01809, https://doi.org/10.1029/2011GL049903.

Ma, J., W. L. Lin, X. D. Zheng, X. B. Xu, Z. Li, and L. L. Yang, 2014: Influence of air mass downward transport on the variability of surface ozone at Xianggelila Regional Atmosphere Background Station, southwest China. *Atmospheric Chemistry and Physics*, **14**, 5311–5325, https://doi.org/10.5194/acp-14-5311-2014.

Mitchell, T. D., and P. D. Jones, 2005: An improved method of constructing a database of monthly climate observations and associated high-resolution grids. *International Journal of Climatology*, **25**, 693–712, https://doi.org/10.1002/joc.1181.

Morrison, H., G. Thompson, and V. Tatarskii, 2009: Impact of cloud microphysics on the development of trailing stratiform precipitation in a simulated squall line: Comparison of one- and two-moment schemes. *Mon. Wea. Rev.*, **137**, 991–1007, https://doi.org/10.1175/2008MWR2556.1.

Nair, V. S., and Coauthors, 2007: Wintertime aerosol characteristics over the indo-gangetic plain (IGP): Impacts of local boundary layer processes and long-range transport. *J. Geophys. Res.*, **112**, D13205, https://doi.org/10.1029/2006JD008099.

Niu, G.-Y., and Coauthors, 2011: The community Noah land surface model with multiparameterization options (Noah-MP): 1. Model description and evaluation with local-scale measurements. *J. Geophys. Res.*, **116**, D12109, https://doi.org/10.1029/2010JD015139.

Rajput, P., M. M. Sarin, D. Sharma, and D. Singh, 2014: Atmospheric polycyclic aromatic hydrocarbons and isomer ratios as tracers of biomass burning emissions in Northern India. *Environmental Science and Pollution Research*, **21**(8), 5724–5729, https://doi.org/10.1007/s11356-014-2496-5.

Ramanathan, V., and Coauthors, 2005: Atmospheric brown clouds: Impacts on South Asian climate and hydrological cycle. *Proceedings of the National Academy of Sciences of the United States of America*, **102**, 5326–5333, https://doi.org/10.1073/pnas.0500656102.

Reddy, R. R., K. R. Gopal, L. S. S. Reddy, K. Narasimhulu, K. R. Kumar, Y. N. Ahammed, and C. V. K. Reddy, 2008: Measurements of surface ozone at semi-arid site Anantapur (14.62°N, 77.65°E, 331 m asl) in India. *Journal of Atmospheric Chemistry*, **59**, 47–59, https://doi.org/10.1007/s10874-008-9094-1.

Seinfeld, J., 2008: Black carbon and brown clouds. *Nature Geoscience*, **1**, 15–16, https://doi.org/10.1038/ngeo.2007.62.

Streets, D. G., K. F. Yarber, J.-H. Woo, and G. R. Carmichael, 2003: Biomass burning in Asia: Annual and seasonal estimates and atmospheric emissions. *Global Biogeochemical Cycles*, **17**(4), 1099, https://doi.org/10.1029/2003GB002040.

Venkataraman, C., G. Habib, A. Eiguren-Fernandez, A. H. Miguel, and S. K. Friedlander, 2005: Residential biofuels in South Asia: Carbonaceous aerosol emissions and climate impacts. *Science*, **307**(5714), 1454–1456, https://doi.org/10.1126/science.1104359.

Venkataraman, C., G. Habib, D. Kadamba, M. Shrivastava, J.-F. Leon, B. Crouzille, O. Boucher, and D. G. Streets, 2006: Emissions from open biomass burning in India: Integrating the

inventory approach with high-resolution Moderate Resolution Imaging Spectroradiometer (MODIS) active-fire and land cover data. *Global Biogeochemical Cycles*, **20**, GB2013, https://doi.org/10.1029/2005GB002547.

Wan, X., S. C. Kang, J. Y. Xin, B. Liu, T. X. Wen, P. L. Wang, Y. S. Wang, and Z. Y. Cong, 2016: Chemical composition of size-segregated aerosols in Lhasa city, Tibetan Plateau. *Atmospheric Research*, **174–175**, 142–150, https://doi.org/10.1016/j.atmosres.2016.02.005.

Wiedinmyer, C., S. K. Akagi., R. J. Yokelson., et al., 2011: The Fire INventory from NCAR (FINN): A high resolution global model to estimate the emissions from open burning. *Geoscientific Model Development*, **4**, 625, https://doi.org/10.5194/gmd-4-625-2011.

Xia, X. G., X. M. Zong, Z. Y. Cong, H. B. Chen, S. C. Kang, and P. C. Wang, 2011: Baseline continental aerosol over the central Tibetan plateau and a case study of aerosol transport from South Asia. *Atmos. Environ.*, **45**, 7370–7378, https://doi.org/10.1016/j.atmosenv.2011.07.067.

Xu, B.-Q., M. Wang, D. R. Joswiak, J.-J. Cao, T.-D. Yao, G.-J. Wu, W. Yang, and H.-B. Zhao, 2009: Deposition of anthropogenic aerosols in a southeastern Tibetan glacier. *J. Geophys. Res.*, **114**, D17209, https://doi.org/10.1029/2008JD011510.

Xu, J. Z., Q. Zhang, X. Y. Li, X. L. Ge, C. D. Xiao, J. W. Ren, and D. H. Qin, 2013: Dissolved organic matter and inorganic ions in a central Himalayan glacier-insights into chemical composition and atmospheric sources. *Environ. Sci. Technol.*, **47**, 6181–6188, https://doi.org/10.1021/es4009882.

Xu, R. G., X. X. Tie, G. H. Li, S. Y. Zhao, J. J. Cao, T. Feng, and X. Long, 2018: Effect of biomass burning on black carbon (BC) in South Asia and Tibetan Plateau: The analysis of WRF-Chem modeling. *Science of the Total Environment*, **645**, 901–912, https://doi.org/10.1016/j.scitotenv.2018.07.165.

Xu, X. D., C. G. Lu, X. H. Shi, and S. T. Gao, 2008: World water tower: An atmospheric perspective. *Geophys. Res. Lett.*, **35**, L20815, https://doi.org/10.1029/2008GL035867.

Yang, J. H., S. C. Kang, Z. M. Ji, and D. L. Chen, 2018a: Modeling the origin of anthropogenic black carbon and its climatic effect over the Tibetan Plateau and surrounding regions. *J. Geophys. Res.*, **123**, 671–692, https://doi.org/10.1002/2017JD027282.

Yang, J. H., S. C. Kang, and Z. M. Ji, 2018b: Sensitivity analysis of chemical mechanisms in the WRF-Chem model in reconstructing aerosol concentrations and optical properties in the Tibetan Plateau. *Aerosol and Air Quality Research*, **18**, 505–521, https://doi.org/10.4209/aaqr.2017.05.0156.

Yang, J. H., Z. M. Ji, S. C. Kang, and L. Tripathee, 2021: Contribution of South Asian biomass burning to black carbon over the Tibetan Plateau and its climatic impact. *Environmental Pollution*, **270**, 116195, https://doi.org/10.1016/j.envpol.2020.116195.

Yao, T. D., J. C. Pu, A. X. Lu, Y. Q. Wang, and W. S. Yu, 2007: Recent glacial retreat and its impact on hydrological processes on the Tibetan Plateau, China, and surrounding regions. *Arctic, Antarctic, and Alpine Research*, **39**(4), 642–650, https://doi.org/10.1657/1523-0430(07-510)[YAO]2.0.CO;2.

Yao, T. D., and Coauthors, 2015: Multispherical interactions and their effects on the Tibetan Plateau's earth system: A review of the recent researches. *National Science Review*, **2**, 468–488, https://doi.org/10.1093/nsr/nwv070.

Yin, X. F., and Coauthors, 2017: Surface ozone at Nam Co in the inland Tibetan Plateau: Variation, synthesis comparison and regional representativeness. *Atmospheric Chemistry and Physics*, **17**, 11293–11311, https://doi.org/10.5194/acp-17-11293-2017.

Yin, X. F., B. de Foy, K. P. Wu, C. Feng, S. C. Kang, and Q. G. Zhang, 2019: Gaseous and particulate pollutants in Lhasa, Tibet during 2013–2017: Spatial variability, temporal variations and implications. *Environmental Pollution*, **253**, 68–77, https://doi.org/10.1016/j.envpol.2019.06.113.

Zaveri, R. A., and L. K. Peters, 1999: A new lumped structure photochemical mechanism for large-scale applications. *J. Geophys. Res.,* **104**, 30 387–30 415, https://doi.org/10.1029/1999JD900876.

Zaveri, R. A., R. C. Easter, J. D. Fast, and L. K. Peters, 2008: Model for simulating aerosol interactions and chemistry (MOSAIC). *J. Geophys. Res.*, **113**, D13204, https://doi.org/10.1029/2007JD008782.

Zheng, J., and Coauthors, 2017: Influence of biomass burning from South Asia at a high-altitude mountain receptor site in China. *Atmospheric Chemistry and Physics*, **17**, 6853–6864, https://doi.org/10.5194/acp-17-6853-2017.